Journal of Materials Chemistry A

PAPER

View Article Online
View Journal | View Issue

Cite this: J. Mater. Chem. A, 2014, 2, 9620

Lead-free thermoelectrics: promising thermoelectric performance in p-type $SnTe_{1-x}Se_x$ system†

Ananya Banik and Kanishka Biswas*

Received 18th March 2014
Accepted 11th April 2014

DOI: 10.1039/c4ta01333f

www.rsc.org/MaterialsA

Lead chalcogenides are the best performers for thermoelectric power generation at mid/high temperatures; however, environmental concern about Pb prevents its use in large-scale thermoelectric applications. SnTe, a Pb-free IV–VI narrow band gap semiconductor, has the potential to be a good thermoelectric material due to its crystal structure and valence band characteristics being similar to those of PbTe. Here, we report the promising thermoelectric performance in high quality crystalline ingots of In-doped $SnTe_{1-x}Se_x$ ($x = 0$–0.15) synthesized by a simple vacuum sealed tube melting reaction. First, we have optimized the lattice thermal conductivity of SnTe by solid solution alloying with SnSe. Resonance level formation in the valence band through In doping along with the increase in the contribution of the heavy hole valence band through solid solution alloying significantly improved the Seebeck coefficient, resulting in a promising ZT of ~0.8 at 860 K in the Pb-free p-type 1.5 mol% In doped $SnTe_{0.85}Se_{0.15}$ sample.

Introduction

Thermoelectric materials can convert waste heat to electrical energy, thus they are expected to play an important role in future energy generation and conversion. The main focus in this field is to develop efficient, stable, environment friendly and inexpensive solid materials.[1–4] The dimensionless thermoelectric figure of merit, ZT, is defined as $ZT = \sigma S^2 T/(\kappa_{lat} + \kappa_{el})$, where σ, S, T, κ_{el} and κ_{lat} are the electrical conductivity, Seebeck coefficient, temperature, electronic thermal conductivity and lattice thermal conductivity, respectively. The recent advances reported in the performance of thermoelectric materials have been achieved mainly through the remarkable decrease in the lattice thermal conductivity *via* phonon scattering by solid solution point defects, second phase nanoprecipitates,[5–7] mesoscale grain boundaries[6–8] and intrinsic bond anharmonicity.[9] However, the κ_{lat} cannot be reduced below the amorphous limit as the phonon mean free path cannot be smaller than the inter atomic distance,[10] but recent reports on Cu_2Se and Cu_2S show that the κ_{lat} could be reduced below the amorphous limit in the super ionic phase.[11] Significant improvement of the power factor (σS^2) coupled with low thermal conductivity is necessary to improve the performance of present thermoelectric materials. Approaches to improve the power factor includes enhancement of the Seebeck coefficient through the formation of resonance level in the electronic bands[12–14] and convergence of degenerate electronic band valleys through alloying and carrier engineering.[15–18]

Lead chalcogenide and its alloys are the best performers for thermoelectric power generation,[1–3,5–7,12,15] however, environmental concern about Pb prevents its use in large-scale thermoelectric applications. Tin telluride (SnTe), a Pb free IV–VI narrow band gap semi-conductor, has the potential to be a good thermoelectric material due to the presence of similar valence band characteristics (light hole and heavy hole valence bands)[19–21] to PbTe. SnTe has received limited attention because of the inability to control its very high carrier concentration (10^{20} to 10^{21} cm^{-3}) which results in low S and high κ_{el}.[21] Intrinsic Sn vacancies are responsible for the high p-type carrier concentration in SnTe.[22] Recently, SnTe has been used to alloy with other metal tellurides such as $AgSbTe_2$ to improve the thermoelectric performance.[23,24] Significant enhancement in the ZT of SnTe synthesized by high energy ball milling and spark plasma sintering have been achieved by the increase in the Seebeck coefficient due to the formation of resonance level in the valence band through In doping.[14]

In SnTe, the energy difference between the light hole valence band (L band) and the heavy hole valence band (Σ band) is ~0.3 eV,[19–21] which is similar to that in PbSe. Earlier investigation based on temperature dependent Hall coefficient measurement of SnTe suggests that the convergence of these two bands occurs

New Chemistry Unit, Jawaharlal Nehru Centre for Advanced Scientific Research (JNCASR), Jakkur P.O., Bangalore 560064, India. E-mail: kanishka@jncasr.ac.in

† Electronic supplementary information (ESI) available: Zoomed PXRD (Fig. S1); electrical conductivity (σ) and Seebeck coefficient (S) of $SnTe_{1-x}Se_x$ (Fig. S2); lattice thermal conductivity (κ_{lat}) of $In_ySn_{1-y}Te_{0.85}Se_{0.15}$ (Fig. S3); thermal diffusivity and heat capacity of $SnTe_{1-x}Se_x$ (Fig. S4), thermal diffusivity, heat capacity and Lorenz number of $In_ySn_{1-y}Te_{0.85}Se_{0.15}$ (Fig. S5); and heating–cooling cycle thermoelectric data for a typical sample (Fig. S6). See DOI: 10.1039/c4ta01333f

at around 700 K.[25] Alloying lead chalcogenide with high band gap alkaline earth chalcogenides (MgTe, SrSe) has been known to decrease the energy difference between L and Σ bands to facilitate the convergence with respect to the temperature, thus resulting in an improved Seebeck coefficient.[17,26] Alloying of SnTe ($E_g \sim 0.18$ eV) with SnSe, which is a high band gap ($E_g \sim 0.9$ eV) semiconductor, may decrease the energy difference of the two valence bands of SnTe, thus facilitating the convergence. Moreover, the thermal conductivity of SnTe can be further decreased by solid solution alloying with SnSe.

Here we present the promising thermoelectric performance in the Pb-free In-doped $SnTe_{1-x}Se_x$ (x = 0–0.15) system synthesized by a simple sealed tube melting reaction. We first optimize the thermal conductivity of SnTe through solid solution alloying with SnSe, then the optimized sample is used for further improvement in the Seebeck coefficient by In doping. Resonance level formation in the valence bands through In doping along with convergence of valence bands through solid solution alloying significantly improved the Seebeck coefficient, resulting in a promising ZT of ~0.8 at 860 K in 1.5 mol% In doped $SnTe_{0.85}Se_{0.15}$.

Experimental section

Reagents

Tin (Alfa Aesar 99.99+ %), tellurium (Alfa Aesar 99.999+ %), selenium (Alfa Aesar 99.999+ %) and indium (Alfa Aesar 99.99+ %) were used for synthesis without further purification.

Synthesis

Ingots (~7 g) of $SnTe_{1-x}Se_x$ and pristine SnTe were synthesized by mixing appropriate ratios of high-purity starting materials of Sn, Se and Te in a quartz tube. The tubes were sealed under vacuum (10^{-5} Torr) and slowly heated to 450 °C over 12 h, then heated up to 900 °C in 5 h, soaked for 10 h, and cooled slowly to room temperature. In doped $SnTe_{1-x}Se_x$ samples were synthesized *via* a similar procedure.

Powder X-ray diffraction

Powder X-ray diffraction for all of the samples were recorded using a Cu Kα (λ = 1.5406 Å) radiation on a Bruker D8 diffractometer.

Electrical transport

Electrical conductivity and Seebeck coefficients were measured simultaneously under a helium atmosphere from room temperature to 873 K on a ULVAC-RIKO ZEM-3 instrument system. The typical sample for measurement had a parallelepiped shape with the dimensions of ~2 × 2 × 8 mm^3. The longer direction coincides with the direction in which the thermal conductivity was measured. Heating and cooling cycles give repeatable electrical properties for a given sample (ESI†).

Hall measurement

Carrier concentrations were determined using Hall coefficient measurements at room temperature with a PPMS system. Four-contact Hall-bar geometry was used for the measurement. At 300 K, we estimated the carrier concentration, n, from the formula: $n = 1/eR_H$, where e is the electronic charge.

Thermal transport

Thermal diffusivity, D, was directly measured in the range 300–873 K by using a laser flash diffusivity method in a Netzsch LFA-457 (see the D *vs.* T data for all samples in ESI†). Coins with ~8 mm diameter and ~2 mm thickness were used in all of the measurements. The temperature dependent heat capacity, C_p, was derived using a standard sample (pyroceram) in LFA457 (see the C_p *vs.* T data for all samples in the ESI†). The total thermal conductivity, κ_{total}, was calculated using the formula, $\kappa_{total} = DC_p\rho$, where ρ is the density of the sample, measured using the sample dimension and mass. The density of the pellets obtained was in the range ~96% of the theoretical density.

Results and discussion

The designing strategy for improving the thermoelectric performance of SnTe is described below as two rational steps. First, the lattice thermal conductivity of SnTe was optimized by solid solution alloying with SnSe. Moreover, solid solution alloying facilitates valence band convergence in $SnTe_{1-x}Se_x$. Finally, the sample having the lowest κ_{lat} has been chosen for further improvement in the Seebeck coefficient through In doping.

Solid solution alloying in $SnTe_{1-x}Se_x$

We have synthesized several compositions of $SnTe_{1-x}Se_x$ (x = 0–0.15) by the vacuum sealed tube melting reaction. Up to 15 mol% of Se incorporation, the solid solution nature was retained in $SnTe_{1-x}Se_x$. Powder X-ray diffraction patterns of the pristine and $SnTe_{1-x}Se_x$ (x = 0.05–0.15) could be indexed on the cubic SnTe structure ($Fm\bar{3}m$ space group) with no other second phase within the detection limits of powder XRD (Fig. 1(a)). The

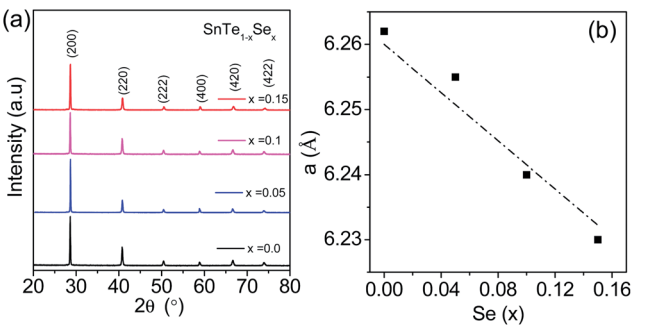

Fig. 1 (a) Powder XRD patterns of $SnTe_{1-x}Se_x$ (x = 0–0.15) samples. (b) Lattice parameter (a) *vs.* Se concentration (x) in $SnTe_{1-x}Se_x$, the dashed line indicates Vegard's law for solid solution.

observed linear contraction in the lattice parameter in $SnTe_{1-x}Se_x$ ($x = 0$–0.15) (Fig. 1(b)) and higher angle shift of the PXRD peak (Fig. S1, ESI†) with increasing Se concentrations indicate the solid solution behavior. The ionic radius of Se (184 pm) is smaller than that of Te (207 pm). As smaller Se is introduced in the place of bigger Te, the unit cell undergoes a systematic contraction, leading to decrease in the lattice parameter. This gradual decrease in the lattice parameter indicates an isomorphic substitution of bigger Te position by smaller Se.

In Fig. 2, we present the temperature dependent total thermal conductivity (κ_{total}) and lattice thermal conductivity (κ_{lat}) of $SnTe_{1-x}Se_x$ ($x = 0$–0.15) samples. The κ_{lat} was obtained after subtracting the electronic part, κ_{el}, from the κ_{total}. The electronic thermal conductivities, $\kappa_e = L\sigma T$, were calculated based on fitting of the respective Seebeck values that estimate the reduced chemical potential from which the Lorenz number, L, can be obtained as explained in detail previously.[27] We present the temperature dependent electrical conductivity (σ) and Seebeck coefficient (S) of $SnTe_{1-x}Se_x$ ($x = 0$–0.15) in the ESI (Fig. S2, ESI†). Significant decrease of κ_{lat} has been achieved in $SnTe_{1-x}Se_x$ ($x = 0.5$–0.15) samples compared to that of pristine SnTe (Fig. 2(b)), which is due to the excess phonon scattering by the solid solution point defects and mass fluctuation. 15 mol% Se incorporated $SnTe_{1-x}Se_x$ has the lowest κ_{lat}, hence the $SnTe_{0.85}Se_{0.15}$ sample has been used for further In doping investigation. Typically, the $SnTe_{0.85}Se_{0.15}$ sample has κ_{lat} of ~1.27 W m^{-1} K^{-1} at 300 K, then it passes through a minima (~0.7 W m^{-1} K^{-1}) at 535 K and reaches ~0.94 W m^{-1} K^{-1} at 710 K (Fig. 2(b)).

We could not resolve the band gap (E_g) of the $SnTe_{1-x}Se_x$ ($x = 0$–0.15) samples by diffuse IR reflectance spectroscopy as the present samples are highly self doped (carriers ~ 10^{20} cm^{-3}) due to intrinsic Sn vacancy. Systematic increase in the E_g has been observed earlier in thin film samples of $SnTe_{1-x}Se_x$ with low carrier concentration.[28] If the energy of the L (light hole) valence band reduced as the band gap increases, which reduces the band offset between L and Σ valence bands in SnTe, the heavy hole Σ band will play a significant role to increase the Seebeck value of the properly doped $SnTe_{0.85}Se_{0.15}$ sample. A similar decrease in the energy difference between L and Σ valence bands in lead chacogenides has been achieved when alloyed with high band gap alkaline earth (Mg/Sr) chalcogenides.[17,26]

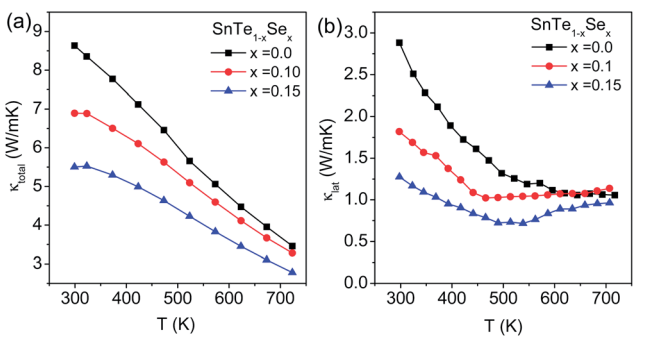

Fig. 2 Temperature-dependent (a) total thermal conductivity (κ_{total}) and (b) lattice thermal conductivity (κ_{lat}) of $SnTe_{1-x}Se_x$ ($x = 0$–0.15).

In doping in $SnTe_{1-x}Se_x$

We have synthesized several In (0–2.5 mol%) doped $SnTe_{0.85}Se_{0.15}$ samples by a similar sealed tube melting reaction. Powder X-ray diffraction patterns of In-doped $SnTe_{0.85}Se_{0.15}$ could be indexed on the cubic SnTe structure ($Fm\bar{3}m$ space group) with no other impurity phase within the detection limits of powder XRD (Fig. 3).

The electrical conductivity (σ) decreases with increasing In concentration up to 2.5 mol%, especially at room temperature from 6110 S cm^{-1} to 1240 S cm^{-1} (Fig. 4(a)). Typically, the room temperature σ of 1.5 mol% In doped $SnTe_{0.85}Se_{0.15}$ is measured to be 1670 S cm^{-1}, which decreases to 640 S cm^{-1} at 855 K, showing a typical degenerate semiconductor behavior. The room temperature Hall coefficients, R_H, of all In doped

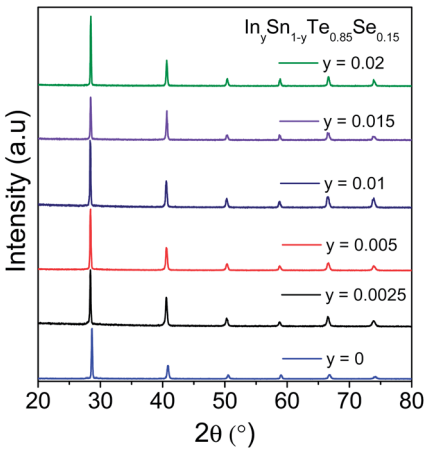

Fig. 3 Powder XRD patterns of $In_ySn_{1-y}Te_{0.85}Se_{0.15}$ samples.

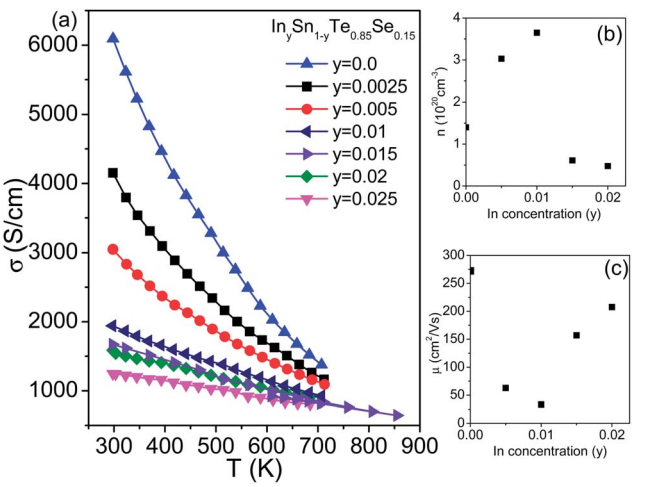

Fig. 4 (a) Temperature dependent electrical conductivity (σ) of $In_ySn_{1-y}Te_{0.85}Se_{0.15}$ samples. (b) Carrier concentration (n) and (c) carrier mobility (μ) at room temperature with respect to In doping concentration (y) in $SnTe_{0.85}Se_{0.15}$.

$SnTe_{0.85}Se_{0.15}$ samples are positive, which indicates the p-type conduction in this system. The carrier concentration (n) at 300 K increases with increasing the In doping concentration up to 1 mol% and then decreases with further increasing the In doping up to 2 mol% (Fig. 4(b)). Indium in IV–VI semiconductors is known to exhibit anomalous behavior, In can act as both a n-type and p-type dopant in IV–VI semiconductor materials.[13] Indium can be present in both monovalent and trivalent forms in IV–VI semiconductors.[13] In the present case, first, In substitutes the Sn in $SnTe_{0.85}Se_{0.15}$ and acts as an acceptor, thus the p-type carrier concentration increases. When the In concentration reaches beyond 1 mol%, extra In atoms act as donors, which decreases the hole carrier concentration in $SnTe_{0.85}Se_{0.15}$.[14] Similar mixed p and n-type doping behavior of In in SnTe has been observed in recently reported In doped SnTe samples.[14] Room temperature hole mobility, defined as $\mu = \sigma/ne$, for various In doped $SnTe_{0.85}Se_{0.15}$ samples is plotted in Fig. 4(c). Decrease in the room temperature σ value with the increase in the In doping concentration is due to the significant decrease in μ. Carrier mobility decreases in In (<1 mol%) doped $SnTe_{0.85}Se_{0.15}$ due to impurity scattering.[14]

Fig. 5(a) presents the temperature dependent Seebeck coefficient (S) data of In (0–2.5 mol%) doped $SnTe_{0.85}Se_{0.15}$ samples. The positive value of S indicates the p-type carriers which supports the Hall measurement. Significant improvement in S has been achieved by In doping in $SnTe_{0.85}Se_{0.15}$, especially at room temperature from ~0.5 μV K^{-1} to ~70 μV K^{-1} with a In doping concentration of 2 mol%. Typically, the room temperature S value measured for 1.5 mol% In doped $SnTe_{0.85}Se_{0.15}$ was ~67 μV K^{-1} which linearly increases to ~175 μV K^{-1} at 855 K.

In Fig. 5(b), we compare the present room temperature S *vs.* n data with previously reported experimental data on In doped SnTe (ball mill + SPS samples),[14] Cu doped SnTe[21] and also with the earlier reported theoretical S *vs.* n curves.[14,19] Theoretical Pisarenko (S *vs.* n) curves at room temperature have been calculated earlier by considering the contribution of both the light hole valence band (L point) and the heavy hole valence band (Σ point). Significant enhancement in the present S values compared to the theoretical Pisarenko plots have been noticed, thus it indicates the creation of resonance level in the valence band of $SnTe_{0.85}Se_{0.15}$ by In doping. Room temperature S values of undoped and Cu-doped samples agree well with the Pisarenko curves.

Fig. 6 presents the temperature dependent power factor (σS^2) data of In (0–2.5 mol%) doped $SnTe_{0.85}Se_{0.15}$ samples. Significant improvement in σS^2 has been achieved mainly due to the enhancement of the thermopower in the present sample. Typically, at room temperature, the σS^2 value for 1.5 mol% In doped $SnTe_{0.85}Se_{0.15}$ is ~7.3 μW cm^{-1} K^{-2}, which rises almost linearly to ~19.2 μW cm^{-1} K^{-2} at ~855 K. Enhancement of σS^2 has been achieved due to the resonance level effect and also due to contribution of the heavy hole valence band especially at high temperature in In doped $SnTe_{1-x}Se_x$.

Indium doping in $SnTe_{0.85}Se_{0.15}$ optimizes the temperature dependent κ_{total} (Fig. 7(a)) by controlling the κ_{el}. Typically, the room temperature κ_{total} value measured for 1.5 mol% In doped $SnTe_{0.85}Se_{0.15}$ is ~2.3 W m^{-1} K^{-1}, which decreases to ~2.15 W m^{-1} K^{-1} at 873 K. $\kappa_{el} = L\sigma T$ was calculated based on fitting of the respective Seebeck values to estimate the reduced chemical potential (η) from which the Lorenz number, L, can be obtained as explained in detail elsewhere.[26] With increasing In doping temperature dependent κ_{el} decreases significantly due

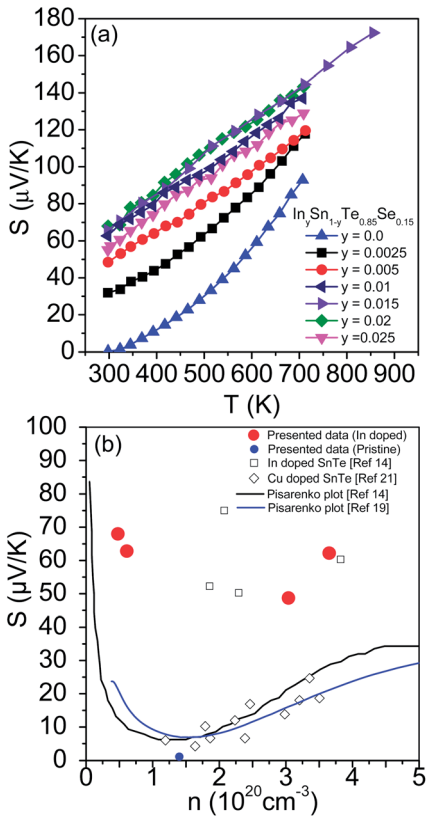

Fig. 5 (a) Temperature dependent Seebeck coefficient (S) of $In_ySn_{1-y}Te_{0.85}Se_{0.15}$ samples. (b) Room temperature S *vs.* n plot of the present $In_ySn_{1-y}Te_{0.85}Se_{0.15}$ samples. For comparison, previously reported S *vs.* n experimental data of In doped SnTe,[14] Cu doped SnTe[21] and theoretical Pisarenko curves[14,19] are given in (b).

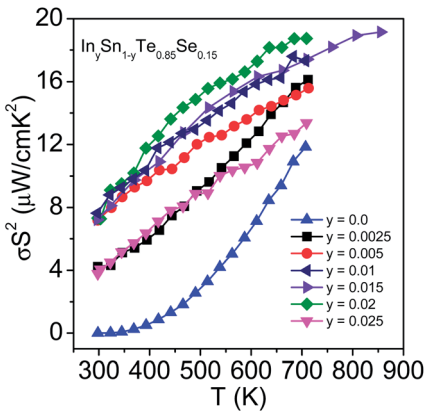

Fig. 6 Temperature dependent power factor (σS^2) of $In_ySn_{1-y}Te_{0.85}Se_{0.15}$ samples.

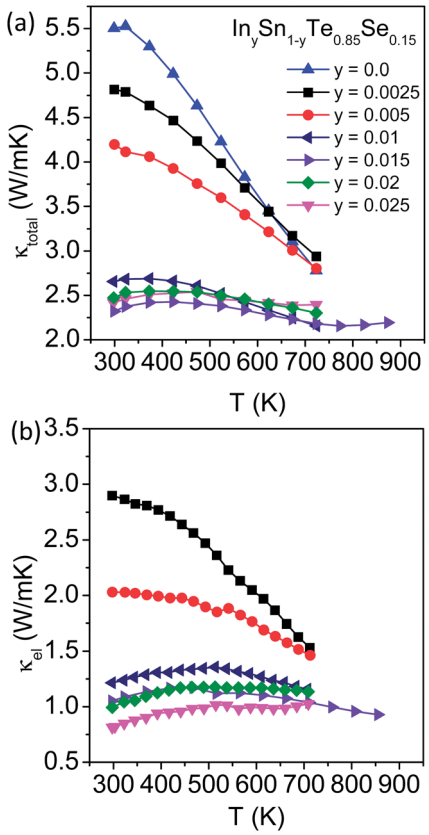

Fig. 7 Temperature-dependent (a) total thermal conductivity (κ_{total}) and (b) electronic thermal conductivity (κ_{el}) of $In_ySn_{1-y}Te_{0.85}Se_{0.15}$ samples. The same symbol notation and colour for the samples is used in all panels.

to the decrease in the temperature dependent σ (Fig. 7(b)). The lattice thermal conductivity, κ_{lat}, was estimated after subtracting the electronic part, κ_{el}, from the κ_{total} (Fig. S3, ESI†).

In Fig. 8 we present temperature dependent ZTs of all In doped $SnTe_{0.85}Se_{0.15}$. The highest ZT value of ~0.8 at 855 K was achieved for 1.5 mol% In doped $SnTe_{0.85}Se_{0.15}$, which is significantly higher compared to undoped SnTe and $SnTe_{0.85}Se_{0.15}$ samples.

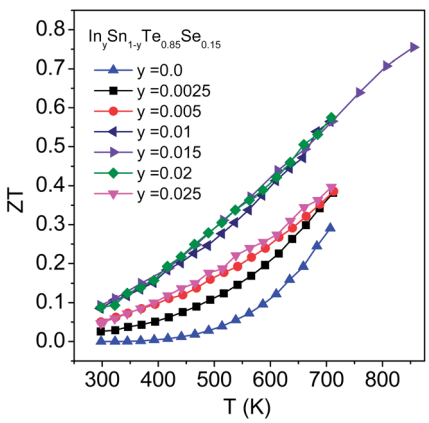

Fig. 8 Temperature-dependent thermoelectric figure of merit (ZT) of $In_ySn_{1-y}Te_{0.85}Se_{0.15}$ samples.

Conclusions

High quality crystalline ingots of In-doped $SnTe_{1-x}Se_x$ (x = 0–0.15) have been synthesized by a simple vacuum sealed tube melting reaction. First, the lattice thermal conductivity of SnTe has been minimized by solid solution alloying with SnSe. Resonance level formation in the valence band through In doping along with convergence of the valence band through solid solution alloying significantly improves the Seebeck coefficient in In doped $SnTe_{1-x}Se_x$, resulting in a enhanced power factor. Improved power factor with relatively low thermal conductivity resulted in a ZT of ~0.8 in the Pb-free $SnTe_{1-x}Se_x$ system. Further improvement in the thermoelectric performance of $SnTe_{1-x}Se_x$ can be achieved through reduction of the thermal conductivity further by second phase nanostructuring and all-scale hierarchical phonon scattering.

Acknowledgements

This work was supported by DST Ramanujan Fellowship, New Chemistry Unit and Sheikh Saqr Laboratory, JNCASR. We thank Mr Somnath Ghara for his help during Hall measurement. We also thank Mr Satya N. Guin for initial help during the experiment.

Notes and references

1 J. Sootsman, D. Y. Chung and M. G. Kanatzidis, *Angew. Chem., Int. Ed.*, 2009, **48**, 8616.
2 L. D. Zhao, V. P. Dravid and M. G. Kanatzidis, *Energy Environ. Sci.*, 2014, **7**, 251.
3 G. J. Snyder and E. S. Toberer, *Nat. Mater.*, 2008, **7**, 105.
4 (*a*) M. Zebarjadi, K. Esfarjani, M. S. Dresselhaus, Z. F. Ren and G. Chen, *Energy Environ. Sci.*, 2012, **5**, 5147; (*b*) Y. Zhang and G. D. Stucky, *Chem. Mater.*, 2014, **26**, 837.
5 K. Biswas, J. He, Q. Zhang, G. Wang, C. Uher, V. P. Dravid and M. G. Kanatzidis, *Nat. Chem.*, 2011, **3**, 160.
6 K. Biswas, J. He, I. D. Blum, C. I. Wu, T. P. Hogan, D. N. Seidman, V. P. Dravid and M. G. Kanatzidis, *Nature*, 2012, **489**, 414.
7 L. D. Zhao, S. Hao, S. H. Lo, C. I. Wu, X. Zhou, Y. Lee, H. Li, K. Biswas, T. P. Hogan, C. Uher, C. Wolverton, V. P. Dravid and M. G. Kanatzidis, *J. Am. Chem. Soc.*, 2013, **135**, 7364.
8 B. Poudel, Q. Hao, Y. Ma, Y. Lan, A. Minnich, B. Yu, X. Yan, D. Wang, A. Muto, D. Vashee, X. Chen, J. Liu, M. S. Dresselhaus, G. Chen and Z. Ren, *Science*, 2008, **320**, 634.
9 D. T. Morelli, V. Jovovic and J. P. Heremans, *Phys. Rev. Lett.*, 2008, **101**, 035901.
10 G. A. Slack, *Solid State Phys.*, 1979, **34**, 1.
11 (*a*) H. Liu, X. Shi, F. Xu, L. Zhang, W. Zhang, L. Chen, Q. Li, C. Uher, T. Day and G. J. Snyder, *Nat. Mater.*, 2012, **11**, 422; (*b*) Y. He, T. Day, T. Zhang, H. Liu,

X. Shi, L. Chen and G. J. Snyder, *Adv. Mater.*, DOI: 10.1002/adma. 201400515.

12 (*a*) J. P. Heremans, V. Jovovic, E. S. Toberer, A. Saramat, K. Kurosaki, A. Charoenphakdee, S. Yamanaka and G. J. Snyder, *Science*, 2008, **321**, 554; (*b*) J. P. Heremans, B. Wiendlocha and A. M. Chamoire, *Energy Environ. Sci.*, 2011, **5**, 5510.

13 S. Ahmad, K. Hoang and S. D. Mahanti, *Phys. Rev. Lett.*, 2006, **96**, 56403.

14 Q. Zhang, B. Liao, Y. Lan, K. Lukas, W. Liu, K. Esfarjani, C. Opeil, D. Broido, G. Chen and Z. Ren, *Proc. Natl. Acad. Sci. U. S. A.*, 2013, **110**, 13261.

15 (*a*) Y. Pei, X. Shi, A. LaLonde, H. Wang, L. Chen and G. J. Snyder, *Nature*, 2011, **473**, 66; (*b*) Y. Pei, H. Wang and G. J. Snyder, *Adv. Mater.*, 2012, **24**, 6125.

16 W. Liu, X. Tan, K. Yin, H. Liu, X. Tang, J. Shi, Q. Zhang and C. Uher, *Phys. Rev. Lett.*, 2012, **108**, 166601.

17 L. D. Zhao, H. J. Wu, S. Q. Hao, C. I. Wu, X. Y. Zhou, K. Biswas, J. Q. He, T. P. Hogan, C. Uher, C. Wolverton, V. P. Dravid and M. G. Kanatzidis, *Energy Environ. Sci.*, 2013, **6**, 3346.

18 S. N. Guin, A. Chatterjee, D. S. Negi, R. Datta and K. Biswas, *Energy Environ. Sci.*, 2013, **6**, 2603.

19 L. M. Rogers, *Br. J. Appl. Phys.*, 1968, **1**, 845.

20 B. A. Efimova, V. I. Kaidanov, B. Y. Moizhes and I. A. Chernik, *Sov. Phys. Solid State*, 1966, **7**, 2032.

21 R. F. Brebrick and A. J. Strauss, *Phys. Rev.*, 1963, **131**, 104.

22 R. F. Brebrick, *J. Phys. Chem. Solids*, 1963, **24**, 27.

23 M. K. Han, J. Androulakis, S. J. Kim and M. G. Kanatzidis, *Adv. Energy Mater.*, 2012, **2**, 157.

24 Y. Chen, M. D. Nielsen, Y.-B. Gao, T. J. Zhu, X. Zhao and J. P. Heremans, *Adv. Energy Mater.*, 2012, **2**, 58.

25 A. A. Andreev, *Sov. Phys. Solid State*, 1967, **9**, 1232.

26 H. Wang, Z. M. Gibbs, Y. Takagiwa and G. J. Snyder, *Energy Environ. Sci.*, 2014, **7**, 804.

27 L.-D. Zhao, S.-H. Lo, J. He, H. Li, K. Biswas, J. Androulakis, C.-I. Wu, T. P. Hogan, D. Y. Chung, V. P. Dravid, I. Todorov, D. Y. Chung and M. G. Kanatzidis, *J. Am. Chem. Soc.*, 2011, **133**, 20476.

28 L. I. Soliman, B. S. Farag, H. A. Zayed and F. M. Shehata, *Indian J. Pure Appl. Phys.*, 2003, **41**, 131.